

Elastic, Conductive, and Mechanically Strong Hydrogels from Dual-Cross-Linked Aramid Nanofiber Composites

Huimin He, Yanran Li, Hongzhen Liu, Yoonseob Kim, Aixin Yan, and Lizhi Xu*

Cite This: *ACS Appl. Mater. Interfaces* 2021, 13, 7539–7545

Read Online

ACCESS |



Metrics & More



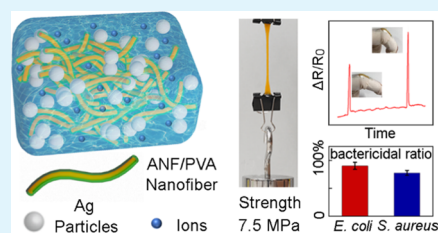
Article Recommendations



Supporting Information

ABSTRACT: Recent research on conductive hydrogels has revealed their potential for building advanced soft bioelectronic devices. Their mechanical flexibility, water content, and porosity approach those of biological tissues, providing a compliant interface between the human body and electronic hardware. Conductive hydrogels could be utilized in many soft tools such as neural electrodes, tactile interfaces, soft actuators, and other electroactive devices. However, most of the available conductive hydrogels exhibit weak mechanical properties, which hinders their application in durable biointegrated systems. Here, we report aramid nanofiber-based hydrogels providing a combination of high elasticity, strength, and electrical conductivity. Highly branched aramid nanofibers (ANFs) provide a robust three-dimensional (3D) framework resembling those in load-bearing soft tissues. When interlaced with poly(vinyl alcohol) (PVA) and cross-linked with both noncovalent and covalent interactions, the nanofiber composites exhibit a high water content of ~76.4 wt %, strength of ~7.5 MPa, ductility of ~407%, and shape recovery of ~99.5% under cyclic tensile stress of 0.3 MPa. Mobile ions impart a conductivity of ~2 S/m to the hydrogels, enabling large-strain sensors with stable operation. In addition, the embedded silver nanoparticles afford broad-spectrum antimicrobial activities, which is favorable for medical devices. The versatility of aramid nanofiber-based composites suggests their further possibilities for functionalization and scalable fabrication toward sophisticated bioelectronic systems.

KEYWORDS: aramid nanofibers, hydrogels, soft electronics, strain sensors, biomimetic composites



INTRODUCTION

Hydrogels represent a class of candidate materials for building soft bioelectronic devices. Unlike the traditional electronics based on rigid components, hydrogels exhibit mechanical flexibility similar to those of soft tissues. Their utilization in bioelectronics could reconcile the interfacial mismatches between natural tissues and the external hardware, enabling conformal tools for biomedical sensing and stimulation.^{1–3} Furthermore, the high porosity and water content of hydrogels could facilitate mass transport for a variety of physiological processes, affording implantable devices compatible with the natural tissues.^{4,5} Although hydrogels were traditionally used as electropassive biomaterials,⁶ recent research has begun to explore conductive hydrogels for building hybrid electronic/ionic devices, with their conductivity realized with mobile ions,^{7,8} conducting polymers,^{9,10} or inorganic fillings.^{11,12} The emerging class of conductive hydrogels created possibilities for soft bioelectronic prototypes, as exemplified by neural electrodes,⁴ tissue scaffolds,^{12,13} soft actuators,⁷ tactile interfaces,^{14,15} and many others.

One of the major challenges for developing hydrogel bioelectronics lies in their mechanical robustness. For instance, typical hydrogels may fracture or permanently deform under low tensile stress at the ~kPa level,^{16–18} which could not afford stable operation under repeated biomechanical loading. Recent strategies for mechanical improvement of hydrogels involve

multiple networks,^{19,20} nanoscale reinforcement,^{21,22} non-covalent cross-linking,^{23,24} dry annealing,⁹ or other physico-chemical treatment.²⁵ However, these methods for hydrogels might compromise their water content, electrical/biochemical functionalities, or processability for hybrid devices. Attaining a set of hydrogel properties desirable for robust bioelectronic tools remains difficult. Developing advanced hydrogel bioelectronics would require additional building blocks, affording a combination of mechanical strength, cyclic stability, and processing routes for electrical and biochemical functions.

We recently developed an approach to biomimetic functional materials based on biocompatible, self-assembled aramid nanofibers (ANFs).^{26,27} The three-dimensional (3D) interconnected ANFs emulate collagen fibrils in load-bearing soft tissues, providing an adaptive and mechanically strong framework for composite hydrogels. When hydrogen bonded with hydrophilic soft polymers, ANF composites could exhibit high mechanical properties while retaining a high water content.²⁸ ANF-based composites could be synthesized with

Received: November 27, 2020

Accepted: January 23, 2021

Published: February 4, 2021



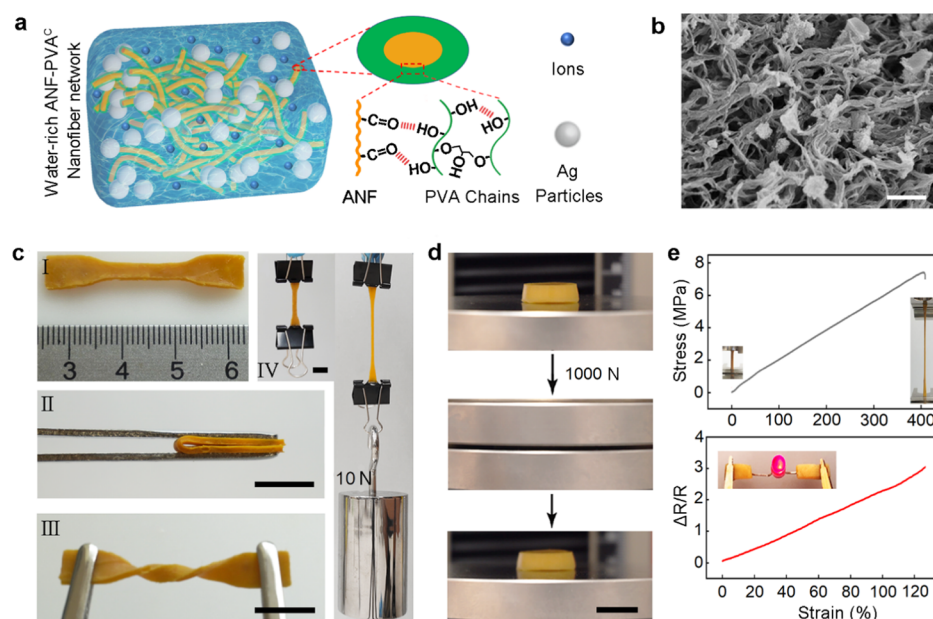


Figure 1. Elastic, conductive, and mechanically strong hydrogels from biomimetic ANF composites. (a) A schematic of ANF-PVA^C-Ag, indicating the ANF/PVA network with both covalent and noncovalent cross-linking, as well as ions and AgNPs dispersed in the hydrogel matrix. (b) A SEM image showing AgNPs embedded in the nanofibrous network. Scale bar: 500 nm. (c) Images of a dumbbell-shaped sample of ANF-PVA^C-Ag (I), and its ability to withstand folding (II), twisting (III), and a tensile load of 10 N (IV). Scale bar: 10 mm. (d) Photographs showing an ANF-PVA^C-Ag sample withstanding a high compressive load and its shape recovery after unloading. Scale bar: 10 mm. (e) The stress–strain curve of ANF-PVA^C-Ag under tension (top), and its fractional change in resistance in response to tensile strain (bottom). The insets demonstrate the ductility and electrical conductivity of ANF-PVA^C-Ag.

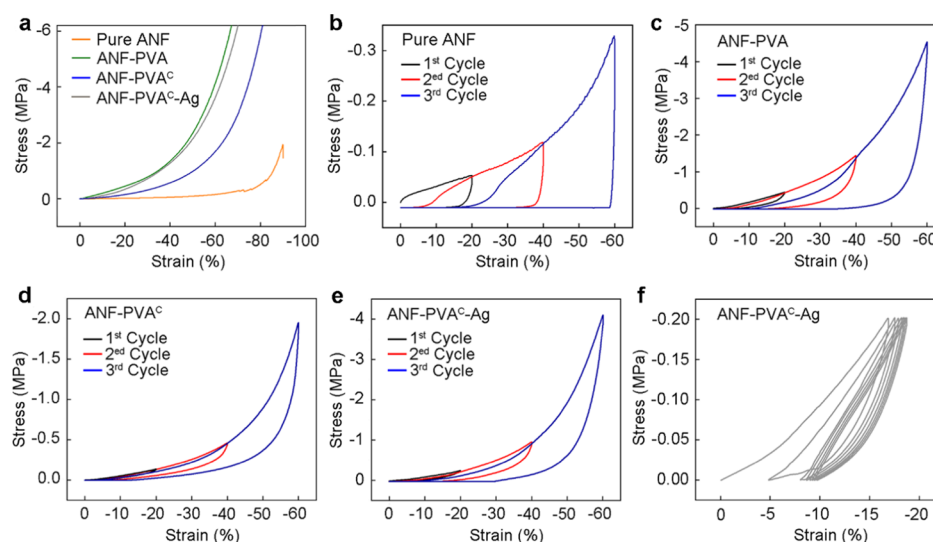


Figure 2. Compression characteristics of various ANF-based hydrogels. (a) Stress–strain curves from unconfined compression tests with a maximum stress of 6.2 MPa. (b–e) Cyclic compression tests for ANF (b), ANF-PVA (c), ANF-PVA^C (d), and ANF-PVA^C-Ag (e) involving three cycles with -20 , -40 , and -60% of strain. (f) A compression test for ANF-PVA^C-Ag involving seven cycles with peak stress of -0.2 MPa.

simple solution-based processes, allowing for integration with many other materials for hybrid devices. Here, we report multifunctional, ANF-based composite hydrogels with a set of properties tailored for bioelectronic applications. With careful cross-linking involving both covalent and noncovalent interactions, these composite hydrogels possess a combination of high elasticity, toughness, and strength to withstand harsh mechanical loadings encountered in wearable systems. Ionic components afford electrical conductivity, enabling large-strain sensors with stable operation under cyclic biomechanical deformation. In addition, silver nanoparticles (AgNPs)

embedded in the composite hydrogels impart broad-spectrum antimicrobial activities. The versatility of ANF-based materials could suggest routes for building advanced soft bioelectronics involving active and durable hydrogel components.

RESULTS AND DISCUSSION

A typical composition of the multifunctional hydrogel involves an ANF framework interlaced with cross-linked poly(vinyl alcohol) (PVA), as well as ions and AgNPs dispersed in a water-rich matrix (Figure 1a). The samples can be prepared based on the solubility differences of ANFs in dimethyl

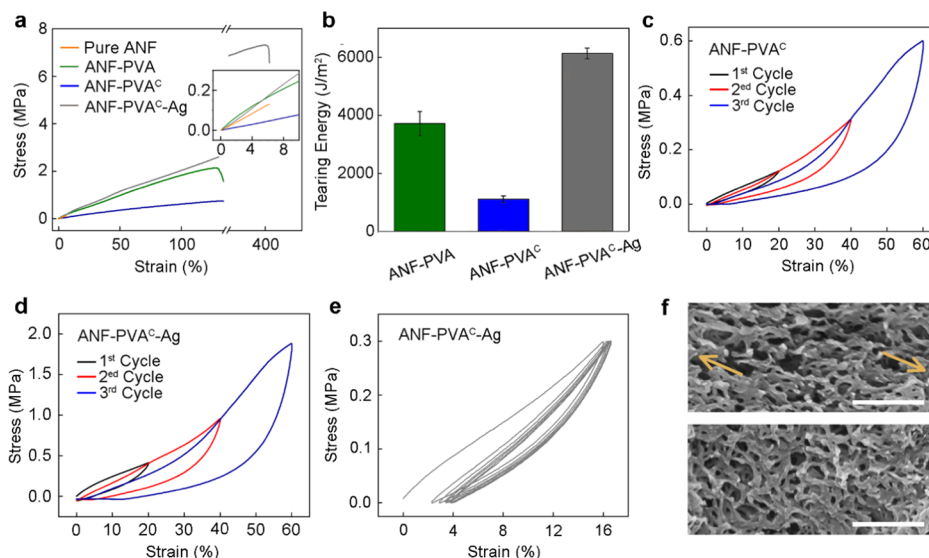


Figure 3. Properties of various ANF-based hydrogels under tension. (a) Uniaxial tensile tests for ANF, ANF-PVA, ANF-PVA^C, and ANF-PVA^C-Ag. The inset shows a magnified plot with low strains. (b) Tearing energy of ANF-PVA, ANF-PVA^C, and ANF-PVA^C-Ag, showing their high toughness. (c, d) Cyclic tensile tests for ANF-PVA^C (c) and ANF-PVA^C-Ag (d) involving three cycles with 20, 40, and 60% of strains. (e) A tensile test for ANF-PVA^C-Ag involving seven cycles with peak stress of 0.3 MPa. (f) SEM images showing a microstructural orientation of ANF-PVA^C-Ag after a loading cycle with 300% of tensile strain (top) and its recovery after resting in water for 2 h. The yellow arrows indicate the direction of tension. Scale bar: 300 nm.

sulfoxide (DMSO) and water (Figure S1). The abundant amide groups on stiff ANFs afford hydrogen bonding with soft PVA chains, enabling effective load transfer through the nanofibrous skeleton and the possibility for structural reconfiguration.²⁸ The PVA chains are covalently cross-linked with epichlorohydrin (ECH), imparting elasticity for the recovery from macroscopic deformation. Ionic components in the hydrogel matrix are introduced during the synthesis process for AgNPs. Briefly, composites involving ANF and cross-linked PVA are soaked in an aqueous solution of silver nitrate (AgNO₃, 1 M in deionized water), a precursor of AgNPs.²⁹ After transferring the samples into an aqueous solution of reducing agents such as sodium citrate (1 M in deionized water), AgNPs could form within the hydrogels (Figure 1b), preferentially in the shallow layers near the surfaces (Figure S2). The content of AgNPs is ~5.2%, as determined by thermogravimetric analysis (Figure S2d). Although there is some loss of Ag particles in the hydrogel surface, the resistance of hydrogels remains consistent in a sodium citrate solution for 7 days as the conductivity is mostly attributed to the mobile ions.

The composite hydrogels exhibit a combination of high mechanical strength, elasticity, and electrical conductivity. Whereas, they retain ~76.4 wt % water, these hydrogels could withstand extreme mechanical loadings and recover to their original undeformed geometry upon the release of the stress (Figure 1c,d; Video S1). The uniaxial tensile test reveals a tensile modulus of ~2.7 MPa, tensile strength of ~7.5 MPa, and ultimate tensile strain of ~407% (Figure 1e), which match or exceed those of load-bearing soft tissues. Furthermore, the composite hydrogels exhibit an electrical conductivity of ~2 S/m, which could be attributed mostly to the mobile ions. AgNPs dispersed in the hydrogel did not form a percolating network and may only have a minor contribution to the electrical conductivity. The resistance of a sample is tested during the tensile process (Figure S3), and the changes in resistance are consistent with the classical effect arising from geometry

changes for hydrogel ionotronics.³⁰ The initial linear part of the relative change of resistance shows an effective gauge factor (GF) of ~2.2 (Figure 1e), indicating further applications in strain sensing.

Comparative studies demonstrate the mechanical properties of the composite hydrogels and their dependence on the material components (Figure 2). We analyze four types of hydrogels with similar weight fractions of ANFs, i.e., pure ANF hydrogels without other solid components (~2.8 wt % solid content), ANF with uncross-linked PVA (ANF-PVA, ~17.6 wt % solid content), ANF with covalently cross-linked PVA (ANF-PVA^C, ~15 wt % solid content), and those with embedded AgNPs (ANF-PVA^C-Ag, ~23.6 wt % solid content). Unconfined compression tests indicate that composites involving PVA possess high compressive strengths of over 6 MPa. Their compressive strength might be associated with water retention by the PVA chains attached to the ANF framework (Figure 2a).²⁸ In contrast, pure ANF hydrogels exhibit a compressive modulus of ~0.17 MPa, bearing low stress of ~0.17 MPa even with ~90% of the compressive strain. We note that the covalent cross-linking might reduce the modulus of ANF-PVA composite hydrogels from ~1.9 to ~0.68 MPa. This effect could be related to the lowered availability of hydroxyl groups on PVA for the hydrogen bonding with ANFs, which may weaken the composite network. This effect is also evidenced by the fact that increasing amount of covalent cross-linking would lead to a higher degree of swelling and a lower modulus for the composite hydrogel (Figures S4 and S5), indicating that the PVA chains are less bonded with the ANFs. Nevertheless, with an optimized amount of covalent cross-linking (~2.5% molar fraction with respect to the hydroxyl groups) (Figure S6), the composite hydrogels retain high compressive strength at the MPa level. In addition, the embedded AgNPs enhance the modulus of the composite hydrogel from ~0.68 to ~1.7 MPa without compromising its strength, which counterbalances the softening effect from the covalent cross-linking. This stiffening

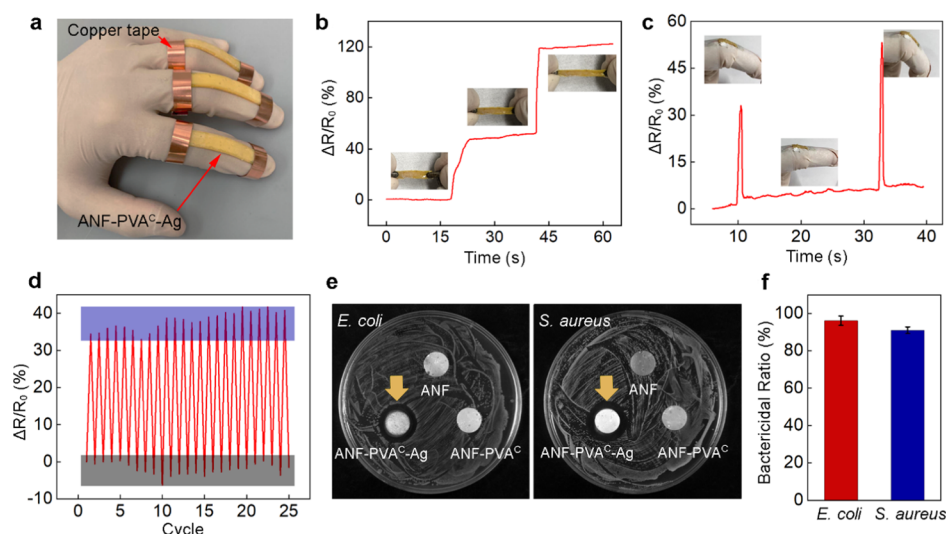


Figure 4. Application of the multifunctional, ANF-based composite hydrogels. (a) An image showing strips of ANF-PVA^C-Ag attached to fingers, serving as resistance-based strain sensors. (b, c) The change of resistance in response to different states of tension for an ANF-PVA^C-Ag strip (b) and its application for characterizing the motion of an index finger (c). (d) Readings of a representative sensor under the cyclic tensile strain of 15%. (e) Images showing bactericidal rings surrounding the ANF-PVA^C-Ag patches on *Staphylococcus aureus* and *Escherichia coli* lawns. (f) The reduction of bacteria counts on ANF-PVA^C-Ag as compared with controls, indicating its broad-spectrum antimicrobial activities.

effect could be attributed to the dense Ag phase and/or deswelling of the hydrogels in ionic solutions. The deswelling of hydrogels may result from the salt-out effect and reduce their water content, which has great influence on their mechanical performance.

Three consecutive compression cycles involving -20 , 40 , and -60% of strain reveal the elasticity of the various samples (Figure 2b–e). The pure ANF barely recovers from large deformation (Figure 2b). Although ANF-PVA exhibits some degree of shape recovery (Figure 2c), its structural integrity mostly relies on noncovalent bonding, which is prone to plastic deformation. For the convenience of discussion, we quantify the shape recovery of samples as the fraction of the maximum strain recovered from a specified loading cycle. In the first cycle, ANF-PVA samples with ~ 17.6 wt % solid content recover $\sim 69.1\%$ of the compressive deformation after the cycle of -20% strain. In second and third cycles, ANF-PVA shows recoverability at ~ 59 and $\sim 46.8\%$, respectively, indicating lower recoverability associated with high compressive deformation. ANF-PVA with 8 wt % solid content recover only 13.7% of the deformation after the -60% strain cycle (Figure S6).

On the other hand, samples involving covalent cross-linking exhibit much greater elasticity under large compressive deformation. ANF-PVA^C could recover 83.7, 85.6, and 82.6% of the compressive deformation from the cycles involving -20 , -40 , and -60% of the strain, respectively (Figure 2d). In contrast to ANF-PVA without cross-linking, the excellent elasticity of ANF-PVA^C has little dependence on the solid content (Figures S6 and S7). The elasticity of ANF-PVA^C is also evidenced by its low water extrusion of ~ 5.1 wt % under a high compressive strain of -80% (Figure S8). On the contrary, pure ANF and ANF-PVA without covalent cross-linking lose ~ 69.2 and ~ 23.5 wt % water under a compressive strain of -80% , respectively. We note that the introduction of AgNPs might slightly reduce the compressive elasticity of the samples (Figure 2e). Nevertheless, under cyclic compressive stress of ~ -0.2 MPa, ANF-PVA^C-Ag exhibits a high shape recovery of

$>95\%$ after the preconditioning of four cycles (Figure 2f). These elastic characteristics under high mechanical loads could be favorable for applications in wearable devices.¹

Tensile and tearing tests further demonstrate the mechanical characteristics of the composite hydrogels (Figure 3). While pure ANF hydrogels fracture at a low tensile strain of $\sim 6.2\%$, samples involving both ANF and PVA show ductility of over 100%. We note that the covalent cross-linking would reduce the tensile modulus from ~ 2.9 MPa for ANF-PVA to ~ 0.8 MPa for ANF-PVA^C (Figure 2a). This effect is consistent with those revealed by the compression tests. On the other hand, inclusion of AgNPs and ions would enhance the tensile modulus of covalently cross-linked samples to ~ 2.7 MPa (ANF-PVA^C-Ag). Furthermore, ANF-PVA^C-Ag exhibits a high tensile strength of 7.4 MPa and an ultimate tensile strain of 407%. Tearing tests reveal a high tearing energy of 6130 J/m² for ANF-PVA^C-Ag, as compared with 3713 J/m² for ANF-PVA and 1106 J/m² for ANF-PVA^C (Figures 3b and S9). These values indicate that the toughness of the composite hydrogels is similar or higher than those of the load-bearing soft tissues, as exemplified by cartilage (~ 1000 J/m²).³¹ While further mechanisms underlying the strengthening and toughening effects with AgNPs are still under investigation, we attribute the high tensile properties of the composite hydrogels to the stiff ANF framework and their reconfigurable hydrogen bonding with soft PVA chains.²⁸

The cross-linking involving both covalent and noncovalent interactions affords tensile elasticity in combination with the high toughness. Under cyclic tensile loads, both ANF-PVA^C and ANF-PVA^C-Ag exhibit excellent shape recovery from large deformation. ANF-PVA^C recovers 92.8, 94.5, and 91.5% from the cycles involving 20, 40, and 60% of tensile strain, respectively (Figure 3c). The percentages of shape recovery for ANF-PVA^C-Ag under tension are 78, 80.4, and 75.2% for the loading cycles involving 20, 40, and 60% of strain (Figure 3d), which are slightly lower than those of ANF-PVA^C. Nevertheless, under cycles involving tensile stress of 0.3 MPa,

ANF-PVA^C-Ag shows shape recovery of >99.5% from the fourth cycle onward (Figure 3e).

Shape recovery of dual-cross-linked samples is further evidenced by microstructural analyses using scanning electron microscopy (SEM). Following a tensile cycle involving 300% of strain, ANF-PVA^C-Ag exhibits an alignment of nanofibers along the direction of tension (Figure 3f). After immersion of the mechanically cycled sample in water for 2 h without stress, the sample recovers toward the undeformed geometry and no longer exhibits orientation of nanofibers along the tensile direction (Figure 3f). This viscoelastic behavior of the nanofiber network is consistent with its chemical moieties and the macromolecular interactions, providing additional capability of time-dependent shape recovery.

The combination of elasticity, strength, and electrical conductivity of ANF-based composite hydrogels suggests their further applications in soft bioelectronics. To demonstrate the functionality, we explored samples of ANF-PVA^C-Ag as sensors for the motion of fingers (Figure 4a). These samples exhibit rapid changes in resistance in response to the applied deformation (Figure 4b). They could capture the motion of an index finger with the amplitude of the motion indicated by the fractional change of resistance (Figure 4c). Due to the high elasticity of the composite hydrogels, the sensors exhibit stable responses under cycles involving 15% of tensile strain (Figure 4d), suggesting their utilities in robust wearable devices.

Furthermore, AgNPs in the composite hydrogel provide antimicrobial potentials. To examine this, we measured the bactericidal activities of AgNPs against representative Gram-positive and Gram-negative bacteria *S. aureus* and *E. coli*, respectively. Hydrogel samples were deposited onto the culture lawns of *S. aureus* and *E. coli*, respectively, for evaluation of their antimicrobial effects. We note that bactericidal rings were observed surrounding the ANF-PVA^C-Ag on both the *S. aureus* and *E. coli* lawns (Figure 4e). Quantitative analysis involves counting of the surviving bacteria cultured on the samples for 1 h. As compared with nonantibacterial ANF-PVA^C, ANF-PVA^C-Ag displayed bactericidal ratios of 96.1 and 91.1% for *E. coli* and *S. aureus*, respectively, indicating its broad-spectrum antimicrobial activity (Figure 4f).

CONCLUSIONS

In conclusion, we have developed an approach to ANF-based multifunctional hydrogels tailored for robust bioelectronic devices. The nanofibrous network involving both covalent and noncovalent cross-linking affords a unique combination of high strength, toughness, and elasticity. When loaded with ionic charge carriers and AgNPs, the composite hydrogels could serve as large-strain sensors with an additional antimicrobial function. The versatility of ANF-based composites suggests further routes for their functionalization toward various biomedical tools, including biochemical sensors, chronic implants, tactile devices, and many others. Techniques for their patterning and integration with other electronic components could enable sophisticated devices for physiological mapping and stimulation, which deserve further research attention.

METHODS/EXPERIMENTAL SECTION

Materials. Aramid fibers (Kevlar) were obtained from DuPont (USA). Poly(vinyl alcohol) (PVA; M_w : 146 000–186 000, 99% + hydrolyzed) was acquired from Sigma-Aldrich (USA). Dimethyl sulfoxide (DMSO) and epichlorohydrin (ECH) were purchased from

Aladdin (China). Silver nitrate and trisodium citrate dihydrate were provided by SHOWA (Japan).

Preparation of ANF-Based Hydrogels. ANF and ANF-PVA hydrogels were prepared by solvent exchange processes described elsewhere.²⁸ Briefly, an aramid nanofiber (ANF) dispersion in basic DMSO and a PVA solution in DMSO were mixed with an optimized weight ratio of 1:5 (0.2 g of ANF in 9.8 g of DMSO was mixed with 1 g of PVA in 9 g of DMSO). Solid hydrogels formed after immersing the molded mixture in an excess amount of deionized water. ANF-PVA^C was synthesized by adding a cross-linker (ECH, an optimized amount of 0.053 g ECH was added into 20 g of the ANF-PVA mixture) into the ANF and PVA mixture in DMSO. The reaction for covalent cross-linking proceeded at room temperature (about 22 °C) for 24 h and the samples were then soaked in deionized (DI) water for 24 h to achieve the ANF-PVA^C hydrogel. For the fabrication of ANF-PVA^C-Ag, the as-prepared ANF-PVA^C hydrogel was first soaked in a AgNO₃ solution (1 M) for 1 h. After that, the Ag⁺-saturated ANF-PVA^C hydrogel was soaked in a reducing agent of a sodium citrate solution (1 M) for another 1 h.

Microstructural and Electrical Characterization. Supercritical CO₂ drying (tousimis Autosamdri 931, USA) was used to prepare samples for SEM characterization. The weight fraction of water or solid content was determined by measuring the weight of the sample before and after drying. The electrical conductivity of hydrogels (σ) was calculated by $\sigma = L/(RA)$, where L is the length of the sample, R is the electrical resistance, and A is the area of the cross section. The electrical resistance was measured using an electrochemical station (CHI 660E, China) at a working current of 0.0001 A.

Mechanical Tests. For compression tests, cylinder-shaped samples with a diameter of about 18 mm and a height of about 8 mm were fixed between two metal plates. The uniaxial compression tests and cyclic compressive tests were performed at a constant rate of 10%/min. For tensile tests, a hydrogel sheet with a thickness of 1.5 mm was cut into dumbbell-shaped samples with a gauge length of 12 mm and a width of 2.5 mm. The samples were mounted on the clamps and stretched under a constant rate of 100%/min. All of the tests were performed using a tensile-compressive tester. (Zwick Roell, German). The tensile/compression modulus was calculated according to the initial slope of strain–stress curves at a strain of $\pm 2\%$. A quantitative metric of elasticity is the shape recovery of samples after cyclic loading (r),^{32,33} which is calculated according to the equation $r = \left(\frac{\varepsilon_x - \varepsilon_y}{\varepsilon_x - \varepsilon_z} \right) \times 100\%$, where ε_x , ε_y , and ε_z represent the maximum strain in the cycle, the residual strain after unloading, and the strain before loading, respectively. Tearing tests were performed to quantify the fracture energy of the hydrogel. Samples (7.5 mm width \times 50 mm length) were cut into a trouser shape with an initial notch length of about 20 mm. The two arms of the sample were mounted on the clamps. The upper clamp was loaded at a constant low velocity of 1.7 mm/s, and the corresponding tearing force F was recorded. The fracture energy Γ was calculated by $\Gamma = 2F/w$, where w is the thickness of the sample and F is the average tearing force when cracks propagate.

Antimicrobial Assay for Hydrogels. The hydrogels used for antimicrobial assay were cut into disk-shaped samples with a diameter of about 10 mm and a thickness of about 1 mm. Samples were rinsed with a 75% ethanol solution before immersing in a phosphate-buffered solution (PBS) overnight. The antibacterial performance of hydrogels was assessed by the presence and size of clear zones that appeared on bacteria lawns. *S. aureus* and *E. coli* suspensions (100 μ L, 1×10^8 CFU/mL) were first evenly spread onto Luria–Bertani (LB) agar plates, respectively. Samples were then placed onto the designated locations. The plates were incubated at 37 °C for 24 h before imaging. For quantitative assay, a bacterial suspension (10 μ L, 5×10^8 CFU/mL) was loaded onto each sample placed at the surface of an LB agar plate. After 1 h of incubation at 37 °C and 95% humidity, samples with loaded bacteria were removed from the agar plate and were suspended in 1 mL of PBS to recover microbial survivors. After 10-fold serial dilutions, 200 μ L of the 10^{-3} , 10^{-4} , 10^{-5} dilutions were plated onto LB agar plates and incubated at 37 °C for 24 h. Colony-

forming units were counted for ANF-PVA^C (control group) and ANF-PVA^C-Ag samples. The bactericidal ratio was calculated by the equation: bactericidal ratio = (CFU of control – CFU of ANF-PVA^C-Ag hydrogel)/CFU of control × 100%. Duplicates were conducted and the results were shown as the mean value.

■ ASSOCIATED CONTENT

Supporting Information

The Supporting Information is available free of charge at <https://pubs.acs.org/doi/10.1021/acsami.0c21148>.

The video showing an ANF-PVA^C-Ag sample withstanding a high compressive load and its shape recovery after unloading (MP4)

Details of the fabrication processes, nanostructures, swelling information, and mechanical properties (PDF)

■ AUTHOR INFORMATION

Corresponding Author

Lizhi Xu – Department of Mechanical Engineering, The University of Hong Kong, Hong Kong SAR 999077, China; orcid.org/0000-0001-6888-0524; Email: xulizhi@hku.hk

Authors

Huimin He – Department of Mechanical Engineering, The University of Hong Kong, Hong Kong SAR 999077, China; orcid.org/0000-0002-9382-3027

Yanran Li – School of Biological Sciences, The University of Hong Kong, Hong Kong SAR 999077, China

Hongzhen Liu – Department of Mechanical Engineering, The University of Hong Kong, Hong Kong SAR 999077, China

Yoonseob Kim – Department of Chemical and Biological Engineering, Hong Kong University of Science and Technology, Hong Kong SAR 999077, China; orcid.org/0000-0002-6892-8281

Aixin Yan – School of Biological Sciences, The University of Hong Kong, Hong Kong SAR 999077, China

Complete contact information is available at: <https://pubs.acs.org/doi/10.1021/acsami.0c21148>

Author Contributions

This manuscript was written through the contributions of all authors. All authors have given approval to the final version of the manuscript.

Notes

The authors declare no competing financial interest.

■ ACKNOWLEDGMENTS

L.X. acknowledges financial support from the Research Grants Council, University Grants Committee (Project numbers: 27210019 and 17200320).

■ REFERENCES

(1) Ray, T. R.; Choi, J.; Bandodkar, A. J.; Krishnan, S.; Gutruf, P.; Tian, L. M.; Ghaffari, R.; Rogers, J. A. Bio-Integrated Wearable Systems: A Comprehensive Review. *Chem. Rev.* **2019**, *119*, 5461–5533.

(2) Someya, T.; Amagai, M. Toward a New Generation of Smart Skins. *Nat. Biotechnol.* **2019**, *37*, 382–388.

(3) Yang, J. C.; Mun, J.; Kwon, S. Y.; Park, S.; Bao, Z.; Park, S. Electronic Skin: Recent Progress and Future Prospects for Skin-Attachable Devices for Health Monitoring, Robotics, and Prosthetics. *Adv. Mater.* **2019**, *31*, No. 1904765.

(4) Liu, Y.; Liu, J.; Chen, S.; Lei, T.; Kim, Y.; Niu, S.; Wang, H.; Wang, X.; Foudeh, A. M.; Tok, J. B. H.; Bao, Z. Soft and Elastic Hydrogel-based Microelectronics for Localized Low-voltage Neuromodulation. *Nat. Biomed. Eng.* **2019**, *3*, 58–68.

(5) Yuk, H.; Lu, B.; Zhao, X. Hydrogel Bioelectronics. *Chem. Soc. Rev.* **2019**, *48*, 1642–1667.

(6) Peppas, N. A.; Hilt, J. Z.; Khademhosseini, A.; Langer, R. Hydrogels in Biology and Medicine: From Molecular Principles to Bionanotechnology. *Adv. Mater.* **2006**, *18*, 1345–1360.

(7) Keplinger, C.; Sun, J. Y.; Foo, C. C.; Rothmund, P.; Whitesides, G. M.; Suo, Z. Stretchable, Transparent, Ionic Conductors. *Science* **2013**, *341*, 984–987.

(8) Jia, M.; Rolandi, M. Soft and Ion-Conducting Materials in Bioelectronics: From Conducting Polymers to Hydrogels. *Adv. Healthcare Mater.* **2020**, *9*, No. 1901372.

(9) Lu, B.; Yuk, H.; Lin, S.; Jian, N.; Qu, K.; Xu, J.; Zhao, X. Pure PEDOT:PSS hydrogels. *Nat. Commun.* **2019**, *10*, No. 1043.

(10) Shi, Y.; Pan, L.; Liu, B.; Wang, Y.; Cui, Y.; Bao, Z.; Yu, G. Nanostructured Conductive Polypyrrole Hydrogels as High-performance, Flexible Supercapacitor Electrodes. *J. Mater. Chem. A* **2014**, *2*, 6086–6091.

(11) Liao, H.; Guo, X.; Wan, P.; Yu, G. Conductive MXene Nanocomposite Organohydrogel for Flexible, Healable, Low-Temperature Tolerant Strain Sensors. *Adv. Funct. Mater.* **2019**, *29*, No. 1904507.

(12) Dvir, T.; Timko, B. P.; Brigham, M. D.; Naik, S. R.; Karajanagi, S. S.; Levy, O.; Jin, H. W.; Parker, K. K.; Langer, R.; Kohane, D. S. Nanowired Three-dimensional Cardiac Patches. *Nat. Nanotechnol.* **2011**, *6*, 720–725.

(13) Mawad, D.; Stewart, E.; Officer, D. L.; Romeo, T.; Wagner, P.; Wagner, K.; Wallace, G. G. A Single Component Conducting Polymer Hydrogel as a Scaffold for Tissue Engineering. *Adv. Funct. Mater.* **2012**, *22*, 2692–2699.

(14) Kim, C.-C.; Lee, H.-H.; Oh, K. H.; Sun, J.-Y. Highly Stretchable, Transparent Ionic Touch Panel. *Science* **2016**, *353*, 682–687.

(15) Larson, C.; Peele, B.; Li, S.; Robinson, S.; Totaro, M.; Beccai, L.; Mazzolai, B.; Shepherd, R. Highly Stretchable Electroluminescent Skin for Optical Signaling and Tactile Sensing. *Science* **2016**, *351*, 1071–1074.

(16) Spencer, A. R.; Primbetova, A.; Koppes, A. N.; Koppes, R. A.; Fenniri, H.; Annabi, N. Electroconductive Gelatin Methacryloyl-PEDOT:PSS Composite Hydrogels: Design, Synthesis, and Properties. *ACS Biomater. Sci. Eng.* **2018**, *4*, 1558–1567.

(17) Tondera, C.; Akbar, T. F.; Thomas, A. K.; Lin, W.; Werner, C.; Busskamp, V.; Zhang, Y.; Minev, I. R. Highly Conductive, Stretchable, and Cell-Adhesive Hydrogel by Nanoclay Doping. *Small* **2019**, *15*, No. 1901406.

(18) Zhang, S.; Chen, Y.; Liu, H.; Wang, Z.; Ling, H.; Wang, C.; Ni, J.; Çelebi-Saltik, B.; Wang, X.; Meng, X.; Kim, H.-J.; Baidya, A.; Ahadian, S.; Ashammakhi, N.; Dokmeci, M. R.; Trivas-Sejdic, J.; Khademhosseini, A. Room-Temperature-Formed PEDOT:PSS Hydrogels Enable Injectable, Soft, and Healable Organic Bioelectronics. *Adv. Mater.* **2020**, *32*, No. 1904752.

(19) Gong, J. Why Are Double Network Hydrogels So Tough? *Soft Matter* **2010**, *6*, 2583–2590.

(20) Sun, J.-Y.; Zhao, X.; Illeperuma, W. R. K.; Chaudhuri, O.; Oh, K. H.; Mooney, D. J.; Vlassak, J. J.; Suo, Z. Highly Stretchable and Tough Hydrogels. *Nature* **2012**, *489*, 133–136.

(21) Nakayama, A.; Kakugo, A.; Gong, J.; Osada, Y.; Takai, M.; Erata, T.; Kawano, S. High Mechanical Strength Double-Network Hydrogel with Bacterial Cellulose. *Adv. Funct. Mater.* **2004**, *14*, 1124–1128.

(22) Rauner, N.; Meuris, M.; Zoric, M.; Tiller, J. C. Enzymatic Mineralization Generates Ultrastiff and Tough Hydrogels with Tunable Mechanics. *Nature* **2017**, *543*, 407–410.

(23) Dai, X.; Zhang, Y.; Gao, L.; Bai, T.; Wang, W.; Cui, Y.; Liu, W. A Mechanically Strong, Highly Stable, Thermoplastic, and Self-

Healable Supramolecular Polymer Hydrogel. *Adv. Mater.* **2015**, *27*, 3566–3571.

(24) Sun, T. L.; Kurokawa, T.; Kuroda, S.; Ihsan, A. B.; Akasaki, T.; Sato, K.; Haque, M. A.; Nakajima, T.; Gong, J. Physical Hydrogels Composed of Polyampholytes Demonstrate High Toughness and Viscoelasticity. *Nat. Mater.* **2013**, *12*, 932–937.

(25) Ye, Y.; Zhang, Y.; Chen, Y.; Han, X.; Jiang, F. Cellulose Nanofibrils Enhanced, Strong, Stretchable, Freezing-Tolerant Ionic Conductive Organohydrogel for Multi-Functional Sensors. *Adv. Funct. Mater.* **2020**, *30*, No. 2003430.

(26) Lyu, J.; Wang, X.; Liu, L.; Kim, Y.; Tanyi, E. K.; Chi, H.; Feng, W.; Xu, L.; Li, T.; Noginov, M. A.; Uher, C.; Hammig, M. D.; Kotov, N. A. High Strength Conductive Composites with Plasmonic Nanoparticles Aligned on Aramid Nanofibers. *Adv. Funct. Mater.* **2016**, *26*, 8435–8445.

(27) Zhu, J.; Yang, M.; Emre, A.; Bahng, J. H.; Xu, L.; Yeom, J.; Yeom, B.; Kim, Y.; Johnson, K.; Green, P.; Kotov, N. A. Branched Aramid Nanofibers. *Angew. Chem., Int. Ed.* **2017**, *56*, 11744–11748.

(28) Xu, L.; Zhao, X.; Xu, C.; Kotov, N. A. Water-Rich Biomimetic Composites with Abiotic Self-Organizing Nanofiber Network. *Adv. Mater.* **2018**, *30*, No. 1703343.

(29) Sun, Y.; Xia, Y. Shape-controlled Synthesis of Gold and Silver Nanoparticles. *Science* **2002**, *298*, 2176–2179.

(30) Yang, C.; Suo, Z. Hydrogel Ionotronics. *Nat. Rev. Mater.* **2018**, *3*, 125–142.

(31) Simha, N. K.; Carlson, C. S.; Lewis, J. L. Evaluation of Fracture Toughness of Cartilage by Micropenetration. *J. Mater. Sci. Med.* **2004**, *15*, 631–639.

(32) Ahn, S. K.; Kasi, R. M. Exploiting Microphase-Separated Morphologies of Side-Chain Liquid Crystalline Polymer Networks for Triple Shape Memory Properties. *Adv. Funct. Mater.* **2011**, *21*, 4543–4549.

(33) Sinha, A.; Mondal, B.; Maji, B. C.; Chattopadhyay, P. P. Enhanced Shape Recovery in Cryogenically Treated Martensitic Ti-Ni Alloys. *Mater. Sci. Eng., A* **2013**, *580*, 273–278.